

A microscale multi-inlet vortex nanoprecipitation reactor: Turbulence measurement and simulation

Janine Chungyin Cheng, Michael G. Olsen, and Rodney O. Fox

Citation: *Applied Physics Letters* **94**, 204104 (2009); doi: 10.1063/1.3125428

View online: <http://dx.doi.org/10.1063/1.3125428>

View Table of Contents: <http://scitation.aip.org/content/aip/journal/apl/94/20?ver=pdfcov>

Published by the [AIP Publishing](#)

Articles you may be interested in

[Reynolds number scaling of coherent vortex simulation and stochastic coherent adaptive large eddy simulation](#)

Phys. Fluids **25**, 110823 (2013); 10.1063/1.4825260

[Stochastic vortex structure method for modeling particle clustering and collisions in homogeneous turbulence](#)

Phys. Fluids **25**, 103301 (2013); 10.1063/1.4824278

[Confocal imaging of laminar and turbulent mixing in a microscale multi-inlet vortex nanoprecipitation reactor](#)

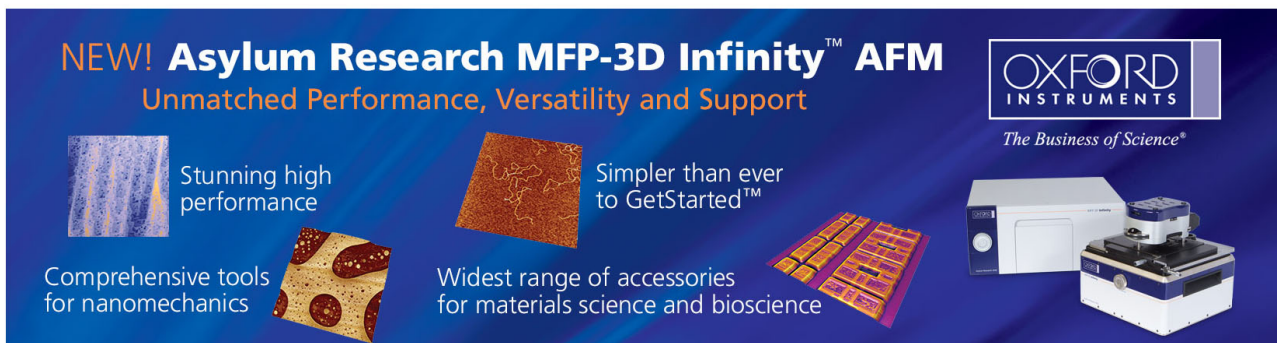
Appl. Phys. Lett. **99**, 204103 (2011); 10.1063/1.3662042

[On particle spin in two-way coupled turbulent channel flow simulations](#)

Phys. Fluids **23**, 093302 (2011); 10.1063/1.3626583

[Large eddy simulation and experimental measurements of the near-field of a large turbulent helium plume](#)

Phys. Fluids **16**, 1866 (2004); 10.1063/1.1689371

The advertisement features a dark blue background with a grid of images showing various AFM scan results. The text is in white and orange. The Oxford Instruments logo is in the top right corner. The main headline is 'NEW! Asylum Research MFP-3D Infinity™ AFM' followed by 'Unmatched Performance, Versatility and Support'. Below this are four key features: 'Stunning high performance' with a scan image, 'Simpler than ever to GetStarted™' with a scan image, 'Comprehensive tools for nanomechanics' with a scan image, and 'Widest range of accessories for materials science and bioscience' with a scan image. On the right, there is a photograph of the MFP-3D Infinity AFM system, including the main unit and a smaller probe head unit.

NEW! Asylum Research MFP-3D Infinity™ AFM
Unmatched Performance, Versatility and Support

OXFORD INSTRUMENTS
The Business of Science®

Stunning high performance

Simpler than ever to GetStarted™

Comprehensive tools for nanomechanics

Widest range of accessories for materials science and bioscience

A microscale multi-inlet vortex nanoprecipitation reactor: Turbulence measurement and simulation

Janine Chungyin Cheng,¹ Michael G. Olsen,^{2,a)} and Rodney O. Fox¹

¹Department of Chemical and Biological Engineering, Iowa State University, Ames, Iowa 50011, USA

²Department of Mechanical Engineering, Iowa State University, Ames, Iowa 50011, USA

(Received 16 February 2009; accepted 27 March 2009; published online 21 May 2009)

Microscale reactors capable of generating turbulent flow are used in Flash NanoPrecipitation, an approach to produce functional nanoparticles with unique optical, mechanical and chemical properties. Microreactor design and optimization could be greatly enhanced by developing reliable computational models of the nanoprecipitation process. A microscale multi-inlet vortex nanoprecipitation reactor was investigated using microscopic particle image velocimetry and computational fluid dynamics. Velocity data such as the mean velocity and turbulent kinetic energy displayed good agreement between experiment and simulation over flow conditions ranging from fully laminar to turbulent, demonstrating the accuracy of the simulation model over the entire turbulent transition range. © 2009 American Institute of Physics. [DOI: 10.1063/1.3125428]

Functional nanoparticles are increasingly important in developing materials for dyes,¹ cosmetics,² pharmaceuticals,^{2–5} and numerous other applications,^{6–8} resulting in great interest in techniques for controlling stability and size range in their production. For example, colloidal drug carriers such as liposomal and micellar dispersions consisting of particles 50–400 nm in diameter have potential use in formulating anticancer therapeutics that can selectively target tumors.⁹

Flash NanoPrecipitation^{10–12}—an approach to produce functional nanoparticles stabilized by amphiphilic copolymer self-assembly—has shown promise for producing nanoparticles for such uses. In addition, nanoparticles encapsulated by copolymer also make it possible to afford long circulations. Ligand-decorated immunoliposomes capable of evading the reticuloendothelial system can be developed using hydrophilic polymer (i.e., polyethylene glycol) stabilization to prevent adsorption of components of the immune system and increase the binding and circulation time.¹³ As illustrated in Fig. 1, Flash NanoPrecipitation employs rapid mixing of solvent and nonsolvent to create high supersaturation to initialize precipitation; rapid mixing uncouples the mixing process from the particle aggregation process and therefore a narrow size range of nanoparticles is attained. This process has been demonstrated in microscale devices such as confined impinging jet reactors (CIJR)^{10,14,15} and multi-inlet vortex reactors (MIVRs).¹⁶ MIVRs are of special interest due to their flexibility in the flow rates of the incoming reactant streams.

An MIVR consists of a cylindrical reaction chamber and four tangentially arranged injectors. At high flow rates, turbulence is generated by the strong collision and redirection of the injected streams. As the injected streams form a swirling vortex pattern instead of an impingement zone (as in a CIJR), an MIVR does not require equal inlet momenta. Thus, the choices of chemicals are more flexible and different intensities of supersaturation can be attained by injecting different amounts of solvent and antisolvent in the inlet streams. The nanoprecipitation is highly dependent on the

fluid dynamics within the reactor. Hence, in order to understand the mixing and nanoprecipitation mechanisms within the MIVR, the flow was investigated using microscopic particle image velocimetry (microPIV), a technique for measuring instantaneous velocity fields in microfluidic devices,¹⁷ and computational fluid dynamics (CFDs). This work represents the first step in developing a reliable computational model for the Flash NanoPrecipitation process in a MIVR capable of predicting output products and therefore improving reactor design and operation.

A schematic of the microPIV experiment is shown in Fig. 2. A microscale MIVR was fabricated with an optical window to allow the light from a frequency doubled neodymium doped yttrium aluminum garnet (Nd:YAG) laser to illuminate 2 μm diameter fluorescent seed particles and for images to be captured with a charge coupled device (CCD) camera attached to an inverted fluorescence microscope. The reactor and channel height was 1.53 mm, the inlet channel width was 1.19 mm, the reactor diameter was 6.26 mm, and the outlet diameter was 1.40 mm. The flow was imaged using a 4 \times 0.13 numerical aperture objective and a 0.45 \times cou-

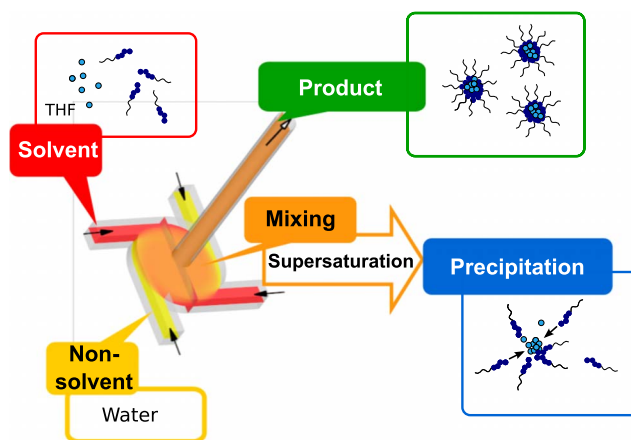


FIG. 1. (Color online) Illustration of MIVR applied to Flash NanoPrecipitation. Drug and polymers are dissolved in solvent and injected to mix with nonsolvent to create supersaturation and therefore precipitate the particles. Protected nanoparticles are obtained after the stabilization by copolymer self-assembly.

^{a)}Electronic mail: mgolsen@iastate.edu.

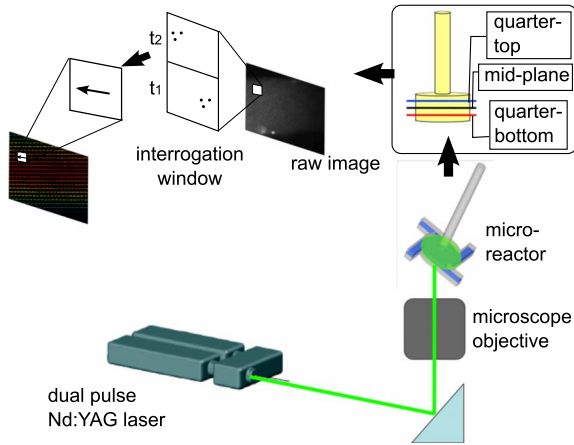


FIG. 2. (Color online) Schematic diagram of micro PIV setup. The reactor was illuminated by a dual pulse Nd:YAG laser and images were captured using a microscope and CCD camera. The images were divided into small interrogation windows and vectors were calculated by correlating two images taken at different times.

pling, resulting in a measurement depth (i.e., *depth of correlation*)^{18,19} of 86 μm and an in-plane vector spacing of 57.6 μm . The fluid used in the experiments was de-ionized water. For each flow condition and location investigated, an ensemble of 1200 velocity field realizations were acquired. Further details of the microPIV system and the experimental methodology can be found in the literature.^{20,21}

The microPIV data were used to evaluate the accuracy of using existing CFD models in simulating the flow within the MIVR. Laminar simulations were performed for low Reynolds number cases, and large eddy simulations (LESs) using the Smagorinsky–Lilly subgrid model^{22,23} were performed for the higher Reynolds number cases. LES was chosen due to its lower computational cost compared to direct numerical simulation. The grid in the simulations consisted of 1 513 324 cells. Three-dimensional simulations were performed using inlet conditions matching those measured in the experiments.

The microPIV data consisted of planes of instantaneous velocity vector fields at three different heights in the reactor: the mid-height of the reactor, and one quarter of a reactor height from the top and from the bottom, as illustrated in Fig. 2. Three sets of microPIV data were collected at each measurement plane corresponding to three different inlet stream Reynolds numbers: $Re_j=53$, $Re_j=93$, and $Re_j=240$. The data were transformed into polar coordinates to obtain tangential and radial velocity components. A comparison between experiment and simulation was accomplished by extracting two-dimensional (2D) planes of data from the CFD simulation results at the locations where the microPIV data were collected. The results are presented here as velocity profiles through the centerline of each of the 2D planes.

For the $Re_j=53$ case, the flow is laminar and the flow patterns at different heights within the reactor chamber are quite distinct. In Fig. 3, the tangential velocity profile indicates that the vortex flow swirls faster at the location closest to the reactor top, suggesting that the flow is mainly influenced by the geometry of the reactor, and also indicating an inhomogeneous mixing area. This increase in tangential velocity is to be expected, as vortex lines are stretched as the flow accelerates toward the exit of the reactor. The radial velocities, shown in Fig. 3, remain negative, indicating a

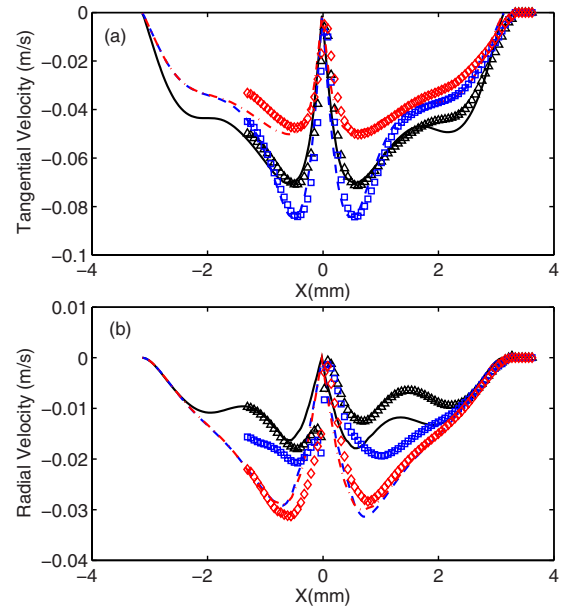


FIG. 3. (Color online) Velocity profile comparison of microPIV and CFD at $Re_j=53$. Data extracted from mid-height of the reactor are represented by Δ , quarter-top plane: \square , quarter-bottom plane: \diamond ; simulation data at corresponding locations are represented by a solid line (mid-plane), dashed line (quarter-top), and dotted line (quarter-bottom).

simple flow pattern where the injected flow is directed to the outlet without much collision and redirection (note that negative radial velocity indicates flow toward the center of the reactor). The tangential and radial velocity components are also roughly of the same order of magnitude, suggesting a poorly developed vortex flow. For this case, good agreement between experiment and simulation was only achieved when the turbulence subgrid model was turned off (i.e., when a laminar simulation was performed).

At $Re_j=93$, the higher observed ratio of tangential to radial velocity indicates a more developed vortex flow. The tangential velocity profiles at different heights shown in Fig. 4 are very close to one another, indicating that there is more homogeneous mixing. The lower tangential velocity at

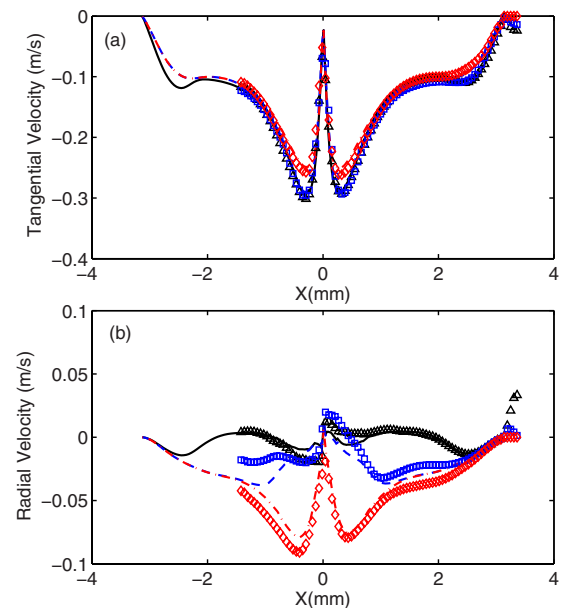


FIG. 4. (Color online) Velocity profile comparison of microPIV and CFD at $Re_j=93$. The symbol description is same as in Fig. 3.

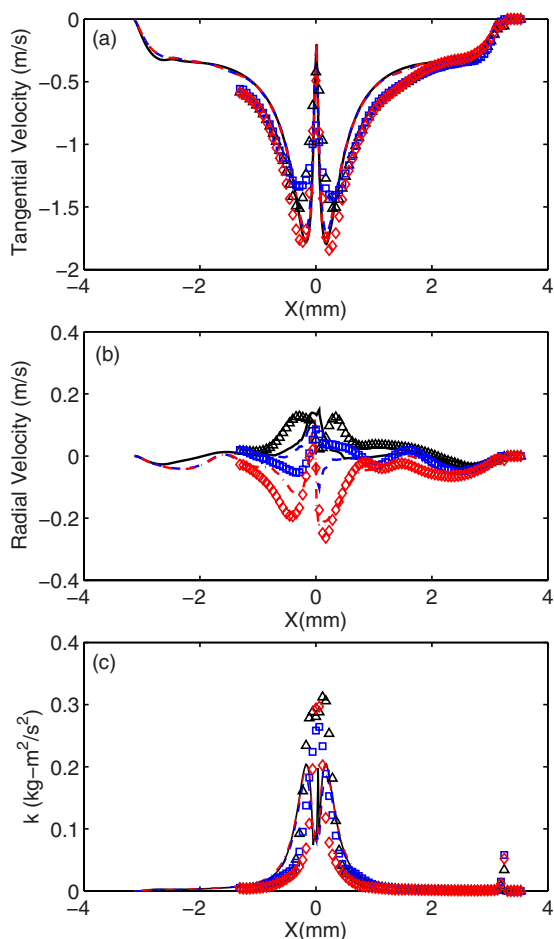


FIG. 5. (Color online) Velocity profile and 2D TKE comparison of microPIV and CFD at $Re_j=240$. The symbol description is same as in Fig. 3.

quarter-bottom than the other two locations suggests the flow is still affected by the geometry; the vortex is not as strong at the bottom of the reactor. The radial velocity profile shown in Fig. 4 differs from the $Re_j=53$ (laminar) case with the presence of non-negative radial velocity at the mid-height plane, indicating a complex flow pattern where the injected streams do not simply swirl inward toward the outlet of the reactor. When this case was modeled by LES (with the turbulence subgrid scale model turned on), good agreement with the experimental results was observed. Note that since the vortex flow is more developed in this case, the radial velocity is an order of magnitude smaller than the tangential velocity, making the radial component more difficult to accurately measure than the tangential component. Thus, the agreement with simulation was not as good as for the tangential velocity.

For the $Re_j=240$ case, the tangential velocity profiles shown in Fig. 5 are close to one another, indicating a homogeneous mixing region. Note that the profile extracted from the top-quarter plane was slightly slower than the other two. This is different from the $Re_j=93$ case, which had a lower tangential velocity at the bottom. This indicates a strong vortex flow where the inlet streams collide and have an extended circulation zone reaching to the reactor bottom. The radial velocities shown in Fig. 5 have a magnitude of only 5% of that of the tangential velocities, indicating a strong vortex flow and also causing difficulty in measuring the radial velocities. For this high Reynolds number, the turbulent

kinetic energy (TKE) was measured for comparison with the simulations. Note that since only planar velocity fields can be obtained using microPIV, only a 2D TKE can be calculated [i.e., $k_{2D}=1/2(u'^2+v'^2)$, where u' and v' are the rms velocity components]. k_{2D} was also calculated from planar velocity fields extracted from the CFD simulations in order to validate the simulation results against the experimental data. The TKE results for the simulations agree well with the experiments except along the axis of the reactor, where the microPIV experiments measure a larger TKE. Because the radial and tangential velocities are small along the reactor axis, k_{2D} should be low at this point. However, the observed TKE at the axis is due not only to turbulent velocity fluctuations, but also due to small unsteady motions of the vortex core resulting from flow instabilities. Unlike the simulations, which can have perfectly constant inlet conditions, there exist small perturbations to the experimental inlet velocity conditions due to the mechanical nature of the gear pumps, and these perturbations result in greater vortex motion, and hence, greater measured TKE at the reactor axis in the experiments.

The work presented here represents the first experimental validation of the accuracy of LES in a microscale nanoprecipitation reactor. The results show that LES is capable of accurately modeling the flow field over the entire turbulent transition range within the microreactor. This finding is an important first step in the development of computer models of the nanoprecipitation process within a microscale MIVR, resulting in a powerful design tool for customizing reactors to produce nanoparticles with desired characteristics.

¹A. J. Gesquiere, T. Uwada, T. Asahi, H. Masuhara, and P. F. Barbara, *Nano Lett.* **5**, 1321 (2005).

²R. H. Muller, M. Radtke, and S. A. Wissing, *Adv. Drug Delivery Rev.* **54**, S131 (2002).

³E. Allemann, R. Gurny, and E. Doelker, *Eur. J. Pharm. Biopharm.* **39**, 173 (1993).

⁴J. E. Kipp, *Int. J. Pharm.* **284**, 109 (2004).

⁵R. H. Muller and K. Peters, *Int. J. Pharm.* **160**, 229 (1998).

⁶A. L. Le Roy Boehm, R. Zerrouk, and H. Fessi, *J. Microencapsul.* **17**, 195 (2000).

⁷E. Romanus, M. Huckel, C. Gross, S. Prass, W. Weitschies, R. Brauer, and P. Weber, *J. Magn. Mater.* **252**, 387 (2002).

⁸Q. Q. Zhao, A. Boxman, and U. Chowdhry, *J. Nanopart. Res.* **5**, 567 (2003).

⁹W. G. Kreyling, M. Semmler, F. Erbe, P. Mayer, S. Takenaka, H. Schulz, G. Oberdorster, and A. Ziesenis, *J. Toxicol. Environ. Health* **65**, 1513 (2002).

¹⁰B. K. Johnson and R. K. Prud'homme, *Aust. J. Chem.* **56**, 1021 (2003).

¹¹B. K. Johnson and R. K. Prud'homme, *Abstr. Pap. - Am. Chem. Soc.* **226**, U487 (2003).

¹²B. K. Johnson and R. K. Prud'homme, *Phys. Rev. Lett.* **91**, 118302 (2003).

¹³O. Ishida, K. Maruyama, K. Sasaki, and M. Iwatsuru, *Int. J. Pharm.* **190**, 49 (1999).

¹⁴B. K. Johnson and R. K. Prud'homme, *AIChE J.* **49**, 2264 (2003).

¹⁵Y. Liu, M. G. Olsen, and R. O. Fox, *Lab Chip* **9**, 1110 (2009).

¹⁶Y. Liu, C. Y. Cheng, Y. Liu, R. K. Prud'homme, and R. O. Fox, *Chem. Eng. Sci.* **63**, 2829 (2008).

¹⁷J. G. Santiago, S. T. Wereley, C. D. Meinhart, D. J. Beebe, and R. J. Adrian, *Exp. Fluids* **25**, 316 (1998).

¹⁸M. G. Olsen and R. J. Adrian, *Exp. Fluids* **29**, S166 (2000).

¹⁹C. J. Bourdon, M. G. Olsen, and A. D. Gorby, *Meas. Sci. Technol.* **15**, 318 (2004).

²⁰H. Li and M. G. Olsen, *ASME Trans. J. Fluids Eng.* **128**, 305 (2006).

²¹H. Li and M. G. Olsen, *Int. J. Heat Fluid Flow* **27**, 123 (2006).

²²V. M. Canuto, *Astrophys. J.* **428**, 729 (1994).

²³P. R. Voke, *Theor. Comput. Fluid Dyn.* **8**, 131 (1996).